AD-A262 798

PL-TR--
92-1054

HIGH STRAIN LAGRANGIAN HYDRODYNAMICS: A THREE-DIMENSIONAL SPH CODE FOR DYNAMIC MATERIAL RESPONSE

DTIC
S ELECTE
C MAR 3 0 1993
D

Firooz A. Allahdadi et al.

March 1993

Final Report

PHILLIPS LABORATORY
Advanced Weapons and Survivability Directorate
AIR FORCE MATERIEL COMMAND
KIRTLAND AIR FORCE BASE, NM 87117-5776

93-06416

93 3 29 072

REPORT DOCUMENTATION PAGE

1. AGENCY USE ONLY (Leave blank)	2. REPORT DATE	3 REPORT TYPE AND DATES COVERED
	March 1993	Final, Oct 91 - Sep 92

4. TITLE AND SUBTITLE

HIGH STRAIN LAGRANGIAN HYDRODYNAMICS: A Three-Dimensional SPH Code for Dynamic Material Response

5 FUNDING NUMBERS

PR: 9993
TA: LA
WU: BS

6. AUTHOR(S)

Firooz A. Allahdadi, Theodore C. Carney,
Jim R. Hipp, Larry D. Libersky, Albert G. Petschek

7. PERFORMING ORGANIZATION NAME(S) AND ADDRESS(ES)

Phillips Laboratory
Kirtland AFB, NM 87117-5776

8. PERFORMING ORGANIZATION REPORT NUMBER

PL-TR--92-1054

9. SPONSORING/MONITORING AGENCY NAME(S) AND ADDRESS(ES)

10. SPONSORING/MONITORING AGENCY REPORT NUMBER

11. SUPPLEMENTARY NOTES

This paper is authored by a team from the Center for Explosives Technology Research at the New Mexico Institute of Mining and Technology, Socorro, NM.; Advanced Sciences Inc, Albuquerque, NM; and the Space Kinetic Impacts and Debris Br, Kirtland AFB, NM.*

12a. DISTRIBUTION/AVAILABILITY STATEMENT

Approved for public release;
Distribution is unlimited.

12b. DISTRIBUTION CODE

13. ABSTRACT (Maximum 200 words)

MAGI, a three-dimensional shock and material response code which is based on Smoothed Particle Hydrodynamics is described. Calculations are presented and compared with experimental results. The SPH method is unique in that it employs no spatial mesh. The absence of a grid leads to some nice features such as the ability to handle large distortions in a pure Lagrangian frame and a natural treatment of voids. Both of these features are important in the tracking of debris clouds produced by hypervelocity impact - a difficult problem for which Smoothed Particle Hydrodynamics seems ideally suited. We believe this is the first application of SPH to the dynamics of elastic-plastic solids.

*Publication of this report does not constitute approval or disapproval of the ideas or findings. It is published in the interest of STINFO exchange.

14. SUBJECT TERMS

Hydrodynamics, numerical, simulations, Lagrangian,
particle, stress, strain.

15. NUMBER OF PAGES

22

16 PRICE CODE

17. SECURITY CLASSIFICATION OF REPORT	18 SECURITY CLASSIFICATION OF THIS PAGE		
Unclassified	Unclassified	Unclassified	SAR

INTRODUCTION

Traditionally, Lagrangian codes have been used to simulate material response when the amount of deformation is small. When the deformation is large, Eulerian calculations have been employed. The Lagrangian calculation is more accurate – the Eulerian calculation has greater applicability. These strengths and weaknesses are due to the convective derivative which is absent in the equations written in the moving Lagrangian frame. Numerical treatment of this advection term is difficult and introduces inaccuracies into the calculation. However, if these errors can be made small, the Eulerian calculation can be used to treat a variety of high strain phenomena.

Various methods have been devised in order to achieve the best features of both approaches. These "hybrid" techniques normally use two grids, one Lagrangian – the other Eulerian, with information exchanged between them. These mappings add a good deal of complexity to the calculation and can also introduce inaccuracies. Nevertheless, many hybrid techniques have been successful and are widely used today

Unique in computational fluid dynamics is Smoothed Particle Hydrodynamics (SPH). This technique uses no underlying grid – it is a pure Lagrangian particle method invented by Lucy [1], Gingold [2,3], Monaghan [4,5,6] and Benz [7]. The absence of a mesh means that large deformations can be computed in a pure Lagrangian frame. It is for this reason that SPH has the potential to be a valuable computational tool. Although SPH has been proven an excellent computational tool for astrophysical applications, its ability to treat typical hydrocode production problems is largely untested at this point. The method is just now being applied to a broad range of problems where its strengths and weaknesses are sure to be exposed.

1

THE METHOD

The foundation of Smoothed Particle Hydrodynamics is interpolation theory. The conservation laws of continuum fluid dynamics, in the form of partial differential equations, are transformed into integral equations through the use of an interpolation function that gives the "kernel estimate" of the field variables at a point. Computationally, information is known only at discrete points, so that the integrals are evaluated as sums over neighboring points. These "interactions" result in a net force which will accelerate the "particle". The reason that an underlying grid is not needed is that functions are evaluated using their value at the discrete points (particles) and an interpolation kernel. An integration by parts then moves spatial derivatives from operating on the physical quantities to operating on the interpolation kernel which is an analytic. These concepts will now be described more fully. Consider a function f, a kernel W which has a width measured by the parameter h, and the following equation:

$$< f(\mathbf{r}) > = \int W(\mathbf{r} - \mathbf{r}', h) f(\mathbf{r}') d\mathbf{r}' \quad . \tag{1}$$

If the integral of W is normalized to unity, then it follows that

$$< f(\mathbf{r}) > \xrightarrow[h \to 0]{} f(\mathbf{r}) \cdot \tag{2}$$

Relation (1) therefore defines the kernel estimate $<f>$ of f. If W is the Dirac delta function then we have the equality $<f>=f$. Now suppose that f is known only at N discrete points that are spatially distributed according to the number density distribution:

$$n(\mathbf{r}) = \sum_{j=1}^{N} \delta(\mathbf{r} - \mathbf{r}_j) \tag{3}$$

If we associate with particle j a volume

2

$$dr' = \frac{m_j}{\varrho(\mathbf{r}_j)} \qquad \text{(4)}$$

thus introducing the concept of particle mass (m), it follows from (1) that

$$< f(\mathbf{r}) > \; \doteq \; \sum_j f_j \; W(\mathbf{r} - \mathbf{r}_j, h) \frac{m_j}{\varrho_j} \qquad \text{(5)}$$

This equation defines a procedure for transforming integral equations to particle equations and is therefore called "integral evaluation by the particle method." A detailed discussion of the theory of SPH is given by Benz [7].

DERIVATION OF THE SPH EQUATIONS

The conservation equations of continuum mechanics are:

$$\frac{d\varrho}{dt} = -\varrho \; \frac{\partial U^\beta}{\partial x^\beta} \qquad \text{(6)}$$

$$\frac{dU^\alpha}{dt} = -\frac{1}{\varrho} \; \frac{\partial \sigma^{\alpha\beta}}{\partial x^\beta} \qquad \text{(7)}$$

$$\frac{dE}{dt} = -\frac{\sigma^{\alpha\beta}}{\varrho} \; \frac{\partial U^\alpha}{\partial x^\beta} \qquad \text{(8)}$$

and $$\frac{dx^\alpha}{dt} = U^\alpha \qquad \text{(9)}$$

Dependent variables are the scalar density (ρ) and specific internal energy (E), the velocity vector velocity U^α, and the stress tensor $\sigma^{\alpha\beta}$. The independent variables are the spatial coordinates (x) and the time (t), and the total time derivative (d/dt) is taken in the moving Lagrangian frame. Summation over repeated greek indicies is implied. Let us now cast equations (6–8) into the SPH framework by applying the procedure outlined above. First, rewrite the momentum and energy equations, so that the density (ρ) appears inside the spatial derivative operator, then find the kernel estimate. The result is

3

$$\int W \frac{d\varrho}{dt} d^3x' = -\int W\varrho \frac{\partial U^\beta}{\partial x'^\beta} d^3x' \qquad . \tag{10}$$

$$\int W \frac{dU^\alpha}{dt} d^3x' = -\int W \frac{\partial}{\partial x'^\beta}\left(\frac{\sigma^{\alpha\beta}}{\varrho}\right) d^3x' - \int W \frac{\sigma^{\alpha\beta}}{\varrho^2} \frac{\partial \varrho}{\partial x'^\beta} d^3x' \qquad . \tag{11}$$

and $$\int W \frac{dE}{dt} d^3x' = -\int W \frac{\sigma^{\alpha\beta}}{\varrho^2} \frac{\partial \varrho U^\alpha}{\partial x'^\beta} d^3x' + \int W \frac{\sigma^{\alpha\beta} U^\alpha}{\varrho^2} \frac{\partial \varrho}{\partial x'^\beta} d^3x' \qquad . \tag{12}$$

We now linearize these equations by taking integrals of products equal to products of integrals (a second order accurate approximation), giving

$$\int W \frac{d\varrho}{dt} d^3x' \approx \varrho(x) \int W \frac{\partial U^\beta}{\partial x'^\beta} d^3x' \qquad . \tag{13}$$

$$\int W \frac{dU^\alpha}{dt} d^3x' \approx -\int W \frac{\partial}{\partial x'^\beta}\left(\frac{\sigma^{\alpha\beta}}{\varrho}\right) d^3x' - \frac{\sigma^{\alpha\beta}(x)}{\varrho^2(x)} \int W \frac{\partial \varrho}{\partial x'^\beta} d^3x' \qquad . \tag{14}$$

and $$\int W \frac{dE}{dt} d^3x' \approx -\frac{\sigma^{\alpha\beta}(x)}{\varrho^2(x)} \int W \frac{\partial \varrho U^\alpha}{\partial x'^\beta} d^3x' + \frac{\sigma^{\alpha\beta}(x) U^\alpha(x)}{\varrho^2(x)} \int W \frac{\partial \varrho}{\partial x'^\beta} d^3x' \qquad . \tag{15}$$

The right-hand-sides of these equations are now integrated by parts, assuming W approaches zero fast enough that the surface terms vanish.

$$\int W \frac{d\varrho}{dt} d^3x' = -\varrho(x) \int U^\beta \frac{\partial W^\beta}{\partial x'^\beta} d^3x' \qquad . \tag{16}$$

$$\int W \frac{dU^\alpha}{dt} d^3x' = -\int \frac{\sigma^{\alpha\beta}(x')}{\varrho(x')} \frac{\partial W}{\partial x'^\beta} d^3x' - \frac{\sigma^{\alpha\beta}(x)}{\varrho^2(x)} \int \varrho(x') \frac{\partial W}{\partial x'^\beta} d^3x' \qquad . \tag{17}$$

and $$\int W \frac{dE}{dt} d^3x' = -\frac{\sigma^{\alpha\beta}(x)}{\varrho^2(x)} \int \varrho(x') U^\alpha(x') \frac{\partial W}{\partial x'^\beta} d^3x' + \frac{\sigma^{\alpha\beta}(x) U^\alpha(x)}{\varrho^2(x)} \int \varrho(x') \frac{\partial W}{\partial x'^\beta} d^3x' . \tag{18}$$

4

Finally, the integrals are evaluated by the particle method, Eq. (5), to give

$$\frac{d\varrho_i}{dt} = -\varrho_i \sum_j \frac{m_j}{\varrho_j} \left(U_i^\beta - U_j^\beta \right) W_{ij,\beta} \qquad . \tag{19}$$

$$\frac{dU_i^\alpha}{dt} = -\sum_j m_j \left(\frac{\sigma_i^{\alpha\beta}}{\varrho_i^2} + \frac{\sigma_j^{\alpha\beta}}{\varrho_j^2} \right) W_{ij,\beta} \qquad . \tag{20}$$

and

$$\frac{dE_i}{dt} = -\frac{\sigma_i^{\alpha\beta}}{\varrho_i^2} \sum_j m_j \left(U_i^\alpha - U_j^\alpha \right) W_{ij,\beta} \qquad . \tag{21}$$

We have introduced the notation $W_{ij} = W(\mathbf{x}_i - \mathbf{x}_j, h)$ and $\partial W_{ij}/\partial x_i^\beta = W_{ij,\beta}$. In obtaining (19) we subtracted from (13) the following term,

$$\varrho_i U_i^\beta \int \frac{\partial W}{\partial x_i^\beta} d^3 x' \doteq \varrho_i U_i^\beta \sum_j \frac{m_j}{\varrho_j} W_{ij,\beta} \qquad , \tag{22}$$

which is zero because the kernel vanishes at infinity. In this way we introduce velocity differences into the density calculation, which is desirable and consistant with the energy calculation in (21). Eqs. (19–21) are the conservation laws of continuum dynamics written in the SPH framework. A given particle i has a density determined by (19), an acceleration obtained from (20) and an internal energy change given by (21). The summations are over neighboring j particles. These equations are not unique. Several other forms of particle equations can be derived using various mathematical manipulations. Some of these are discussed by Monaghan [8].

THE DENSITY CALCULATION

It is important to recognize that (19) is not the density calculation that normally appears in the SPH literature. It is more in the spirit of Smoothed Particle Hydrodynamics to compute the density using the equation obtained by substituting ρ for $<f>$ in (5), namely

5

$$\varrho_i = \sum_j m_j W_{ij} \quad .$$ (23)

With this equation only particle coordinates and masses are required to compute the density, and the continuity equation (6) is automatically satisfied. The disadvantage of using (23) is edge effects – particles near a free surface appear underdense and therefore in tension, causing motion. Benz [7] discusses several possible solutions to this problem including spacing modification, ghost particles, and initial relaxation and the use of (19). It is worthy to note that differentiation of (23) leads to

$$\frac{d\varrho_i}{dt} = -\varrho_i \sum_j \frac{m_j}{\varrho_i} \left(U_i^\beta - U_j^\beta \right) W_{ij,\beta}$$ (24)

which differs from (19) only in that ϱ_i appears in the denominator rather than ϱ_j. We have not yet explored the consequences of using (24) in place of (19). The difference is of the same order as the difference between the product of the expected values and the expected value of the product.

ARTIFICIAL VISCOSITY & WALL HEATING

As they stand, Eqs. (19-21) yield large unphysical oscillations near shocks. In fact, any numerical solution of the continuum equations will exibit this behavior because the dissipative terms have been omitted. Variations of physical quantities across shocks in nature are far to sharp to be captured by numerical techniques. Von Neumann and Richtmyer [9] invented "artifical viscosity" which acts to smooth shocks over a few resolution lengths and stabilize numerical solutions. The additional term is introduced into the equations as an artifical viscous pressure Π. We follow Monaghan and Gingold [4] who derived the following artificial viscous pressure for SPH:

$$\Pi_{ij} = \begin{cases} \dfrac{-\alpha \bar{c}_{ij}\mu_{ij} + \beta\mu_{ij}^2}{\bar{\varrho}_{ij}} & \text{if} \quad (\vec{u}_i - \vec{u}_j)\cdot(\vec{r}_i - \vec{r}_j) < 0 \\[2ex] 0 & \text{otherwise} \end{cases} \tag{25}$$

where

$$\mu_{ij} = \frac{h(\vec{u}_i - \vec{u}_j)\cdot(\vec{r}_i - \vec{r}_j)}{(\vec{r}_i - \vec{r}_j)^2 + \epsilon h^2} \tag{26}$$

and

$$\bar{c}_{ij} = (c_i + c_j)/2 \qquad \bar{\varrho}_{ij} = (\varrho_i + \varrho_j)/2 \quad . \tag{27}$$

The three parameters appearing in these equations have typtical values of α=0.5, β=1.0 and ϵ=0.1. The linear term in (25) uses the sound speed (c). This artifical viscosity gives satisfactory results in most cases, but under some severe conditions it fails to remove spurious heating. An example of this is when a stream of gas is brought to rest against a rigid wall. Noh [10] was able to improve numerical solutions in such cases dramatically by adding an artificial heat conduction term to the energy equation. Monaghan [11] derived the SPH analog of Noh's "wall heating" term in which the net artifical heat flux at particle i is given by

$$H_i = 2\sum_j \frac{\bar{\xi}_{ij}}{\bar{\varrho}_{ij}} \frac{E_i - E_j}{r_{ij}^2} \mathbf{r}_{ij}\cdot\nabla_i W_{ij} \tag{28}$$

where

$$\zeta = g_1 hc + g_2 h^2(|\nabla\cdot\mathbf{v}| - \nabla\cdot\mathbf{v}) \quad , \tag{29}$$

and

$$\bar{\xi}_{ij} = (\zeta_i + \zeta_j)/2 \qquad \bar{\varrho}_{ij} = (\varrho_i + \varrho_j)/2 \quad . \tag{30}$$

Suitable values of the two parameters appearing in (29) are $g_1 = 0.5$ and $g_2 = 1.0$.

CONSTITUTIVE RELATIONS

The stress tensor apperaring in Eqs. (20) and (21) is defined in terms of an isotropic part which is the pressure (P) and the traceless symmetric deviatoric stress (S):

$$\sigma^{\alpha\beta} = P\delta^{\alpha\beta} - S^{\alpha\beta} \qquad . \qquad (31)$$

The pressure is normally computed using an equation of state having functional form $P=P(\rho,E)$, such as the Mie–Gruneisen equation for solids and gamma–law for gases.

$$\textit{Mie--Gruneisen} \qquad P = P_H(1 - \Gamma'\eta) + \Gamma'\varrho E \qquad (32)$$

$$P_H = \begin{cases} a_o\eta + b_o\eta^2 + c_o\eta^3 & \eta > 0 \\ \\ a_o\eta & \eta < 0 \end{cases}$$

$$\textit{Ideal Gas} \qquad P = (\gamma - 1)\varrho E \qquad (33)$$

The subscript "H" refers to the Hugoniot curve, while $\eta=\rho/\rho_o-1$ is used to represent the compression and $\Gamma'=\Gamma\rho/\rho_o$. For the anisotropic part of (31) we write a prognostic equation for the deviatoric stress assuming small displacements

$$\dot{S}^{\alpha\beta} = \mu \overline{\dot{\epsilon}}^{\alpha\beta} = \mu\left(\dot{\epsilon}^{\alpha\beta} - \tfrac{1}{3}\delta^{\alpha\beta}\dot{\epsilon}^{\gamma\gamma}\right) \qquad , \qquad (34)$$

where μ is the shear modulus and $\dot{\epsilon}$ is the traceless rate of strain. However, for finite displacements this equation is not material frame indifferent [12] , that is, the material response will depend in an unphysical way on rotations (and possibly translations) of the material and of the observer describing it. A variety of frame indifferent stress rates have been formulated. Herrmann [13] examines the relative merits of several of these. The Jaumann rate is the most widely used in codes and we adopt it also. With the Jaumann rate, our constitutive equation is

8

$$\dot{S}^{\alpha\beta} - S^{\alpha\gamma}R^{\beta\gamma} - S^{\gamma\beta}\dot{R}^{\alpha\gamma} = \mu\dot{\epsilon}^{\alpha\beta} \qquad (35)$$

The strain rate and rotation rate tensors that have been used are defined as follows:

$$\dot{\epsilon}^{\alpha\beta} = \frac{1}{2}\left(\frac{\partial U^{\alpha}}{\partial x^{\beta}} + \frac{\partial U^{\beta}}{\partial x^{\alpha}}\right) \qquad \dot{R}^{\alpha\beta} = \frac{1}{2}\left(\frac{\partial U^{\alpha}}{\partial x^{\beta}} - \frac{\partial U^{\beta}}{\partial x^{\alpha}}\right) \qquad (36)$$

Particle equations for (35) are obtained by Libersky and Petschek [14] in a manner similar to that of (19,20,21)

$$\frac{dS_i^{\alpha\beta}}{dt} - S_i^{\alpha\beta}\dot{R}_i^{\beta\gamma} - S_i^{\gamma\beta}\dot{R}_i^{\alpha\gamma} = \frac{\mu}{2}\sum_j \frac{m_j}{\varrho_j}\left[\left(U_j^{\alpha} - U_i^{\alpha}\right)W_{ij,\beta} + \left(U_j^{\beta} - U_i^{\beta}\right)W_{ij,\beta} - \frac{1}{3}D_i\delta^{\alpha\beta}\right] \qquad (37)$$

The divergence is already determined by (19), $D_i = -\dot{\varrho}_i/\varrho_i$, and the rotation rate is

$$\dot{R}_i^{\alpha\beta} = \left[\left(U_j^{\alpha} - U_i^{\alpha}\right)W_{ij,\beta} - \left('U_j^{\beta} - U_i^{\beta}\right)W_{ij,\alpha}\right] \qquad (38)$$

The plastic flow regime is determined by the von–Mieses criterion when the second stress invariant $J^2 = S^{\alpha\beta}S^{\alpha\beta}$ exceeds the known flow stess (Y_o). The individual deviators are then brought back to the flow surface.

$$S^{\alpha\beta} = S^{\alpha\beta}\sqrt{\frac{Y_o^2/3}{J^2}} \qquad (39)$$

A more accurate treatment for most metals, not yet implemented in our code, is obtained by computing a history sensitive flow stress, rather than a predetermined fixed value described above. The Johnson–Cook model [15], for example, takes into account thermal softening, strain harding and strain rate effects on the equivalent flow stress. This more sophisticated model contains seven strength related parameters. The elastic–perfectly plastic constitutive model described above contains two parameters, the shear modulus (μ) and the plastic yield stress (Y_o).

THE KERNEL

The interpolation kernel or smoothing function most widely used in SPH is the B-spline W_4.

$$W_4(v,h) = \frac{1}{\pi h^3} \begin{cases} \frac{15}{7}\left(\frac{2}{3} - v^2 + \frac{1}{2}v^3\right) & 0 < v < 1 \qquad v = |r_i - r_j|/h. \\ \frac{5}{14}(2-v)^3 & 1 < v < 2 \\ 0 & \textit{otherwise} \end{cases} \tag{40}$$

The fractional coefficients appearing in (40) assure proper normalization and continuity. This kernel interpolates to second order in h and is always positive in the range of interest. The kernel also has compact support, that is, it goes to zero at a distance $2h$ from its peak. This provides a clear limit on the number of neighbor particles. A Gaussian kernel is second order accurate and positive definite, but the lack of compact support necessitates an artificial cut-off, often taken at $v=3$, making it less a less efficient choice. Higher order interpolation kernels exist [5] but are not always positive definite.

TIME INTEGRATION

Eqs. (19,20,21,37) are integrated using a standard leap-frog algoritihm [16] with time step δt, calculated from the configuration at time t, tc advance the field variabled to $t + \delta t$. We will switch from superscript tensor indicies to subscripts here in order to accomodate the standard superscript representation of the time stepping in which n indicates the current time t and $n + 1$ indicates the advanced time $t + \delta t$.

$$\varrho^{n+1} = \varrho^n(1 - D\delta t) \tag{41}$$

$$U_a^{n+\frac{1}{2}} = U_a^{n-\frac{1}{2}} + \frac{1}{2}(\delta t^n + \delta t^{n-1})F \tag{42}$$

$$E^{n+1} = E^n + \delta t^n G \tag{43}$$

$$S_{\alpha\beta}^{n+1} = S_{\alpha\beta}^n + \delta t^n H \tag{44}$$

$$x_a^{n+1} = x_a^n + U_a^{n+\frac{1}{2}}\delta t^n \tag{45}$$

In these equations F, G and H represent the total acceleration of, work per unit mass and stress rate on a particle as determined by the interactions with neighbor particles. The accuracy of the leap-frog scheme is second order in time and its stability is guaranteed by using the CFL condition to determine the size of the time step δt. We find the minimum over all particles of $\omega h/(c+s)$, where c is the adiabatic sound speed, s is the particle speed, h is the smoothing length and ω a constant factor. Choosing $\omega = 0.3$ seems adequate.

CODE ARCHITECTURE

MAGI differs from most codes in that it was designed from the beginning for application to very large problems on vector supercomputers. Strategies for the efficient implementation of the SPH method were considered and implemented throughout the design and coding of MAGI. Vectorization, an efficient neighbor searcher, accomodation for the symmetry of the particle interactions, and activity flags were all exploited for efficiency and reduced computation.

Activity flags, which mark particles experiencing motion or acceleration are used to gain efficiency. Only active particles and those within a two smoothing lengths of active particles need to be updated. Stationary, unshocked material remains inactive until impacted by moving material or accelerated by a shock or stress wave. This capability results in significant savings in computer time for problems that contain a large number of particles that are initially unaffected by the impact.

11

MAGI consists of a group of subroutines, partitioned by task, that are called in logical sequence each computational cycle. They accomplish the following tasks that are basic to the SPH algorithm. (1) Compute the particle interaction sums on each particle to determine the accelerations, strain rates, and energy increment. (2) Update the velocities, energies, stresses, and density on each particle. (3) Update the pressure on each particle using the new density and energy. (4) Advance the particle positions. The subroutines that perform most tasks consist of a single FORTRAN DO loop that is easily vectorized. The interaction subroutine, however, is an exception. It consists of nested loops, an outer unvectorized loop over all active particles, and two inner loops that are indexed over the list of neighbors that is returned by the linked list described below. Each of the inner loops is vectorized. In the first, the interaction contributions of particle j are summed to particle i. The second updates particle j by contributions from particle i.

The particle interactions themselves are ordered through a linked–list [17] which efficiently determines the neighbor particles contributing to the forces on each particle. Only those neighbor particles within the compact support of the smoothing function need to be considered. The n^2 interactions that result from direct application of the SPH formalism, without consideration of the finite support of the smoothing function, are reduced to order $n \, log \, n$ interactions by means of the linked–list. The interaction lists are further reduced in length by taking advantage of the symmetry in the interactions and the activity flags. Reflective boundaries are incorporated through the linked–list routines by means of "ghost" particles, which are fictitious particles introduced just outside the computational domain to balance the forces on boundary particles and mimic the effect of perfectly reflecting boundaries. Outflow boundaries have also been implemented.

The basic linked list algorithm is composed of two separate routines. The first routine performs several book–keeping functions and is executed only once per problem cycle (time

12

step). This routine begins by calculating a box number for each particle based on its position and the position of a regular grid overlaid on top of the computational domain (the area or volume that bound the computational perimeter) if the particle is within twice the smoothing length ($2h$) of the computational boundary. Finally, a box-ordered linked-list is assembled containing all particles (real and ghost) in order of increasing box number. The number of particles in each box and the box offset (first position) in the linked-list are also stored. The box-ordered linked-list, box offsets, and number of particles per box are used in the second routine described below.

The second subroutine is used to find all nearest neighbors for particle i in the hydrodynamic calculation loop which are subsequently returned in a nearest neighbor linked-list. This is accomplished by looping over all particles contained in the adjacent boxes (defined in the box-ordered linked-list) that surround the box containing particle i. If the nearest neighbor index, j, for one of these particles is greater than i (ij-ji symmetry), and either particle i or j is active, then particle j is tested for interaction proximity to particle i. If all of these conditions are true ($j>i$, i or j active, and $|r_i - r_j| < 2h$), then particle j is added to the nearest neighbor linked-list of particle i.

CALCULATIONS

The Noh Problem – The uniform implosion of an ideal ($\gamma = 5/3$) gas was conceived by Noh [10] as a stringent test problem for shock codes. Initially, the gas is moving radially inward at unit speed, unit density and zero internal energy. Noh found the analytic solution to be a shock moving radially outward at speed 1/3. In spherical geometry the gas behind the shock has particle speed 0, specific internal energy 1/2 and density 64. The value of 64 is due to a 16-fold increase from adiabatic compression and a 4-fold increase across a strong shock for a monatomic gas. Our calculation used one-eighth of a sphere in three-dimensional Cartesian coordinates and three reflecting planes. Particles were placed within this domain in a regula.

cubic array and then randomly perturbed with maximum excursion of $h/8$. The initial radius of the particle cloud was 70. The smoothing length was set to 1 with 1 particle-per-h in each coordinate direction giving roughly 200,000 particles, including ghost particles. Each particle was given unit density, unit speed inward and zero internal energy. Results of the SPH calculation are shown in Figure 1a where the density is plotted as a function of radius for each particle at time = 48. Notice that all SPH particles fall on one curve showing that perfect symmetry is achieved in the calculation. This is the result to be expected as there is no spatial mesh which can bias the solution along gridlines. The shock is in the right place and the density dip (energy spike) near the origin is kept small by the Noh wall-heating term. The calculation took 8 hours to run on a CRAY2 machine. This is a relatively long time, we suspect, compared to other methods. The reason for the slowness is due to the implosion nature of the problem coupled with our linked-list neighbor algorithm. As the gas continues to move radially inward, the calculational time increases dramatically as the number of interacting neighbors for each particle increases from 32 to 2000 because the particles are piling up near the origin but the smoothing length remains fixed. An SPH calculation with variable smoothing length [18] would prove much more efficient for this problem. For explosions and rarefactions the variable smoothing length is often required in order to maintain resolution in an expanding particle cloud. We also present results of the "cylindrical" Noh problem in Figure 1b. In this geometry the gas behind the shock has particle speed 0, specific internal energy 1/2 and density 16. The calculation was run to time = 60 in two-dimensional Cartesian coordinates and required 10,000 particles and 30 minutes of CRAY2 time.

Cylinder Impact Test – Numerical simulation of the deformation of a metal cylinder resulting from normal impact against a flat, rigid surface is often used to test constitutive models in codes. There is ample experimental data and the tests are simple yet stringent. We have modeled an ARMCO Iron cylinder with speed 221 m/s impacting a perfectly reflecting surface using SPH. One-quarter of the cylinder and two reflecting planes were used to
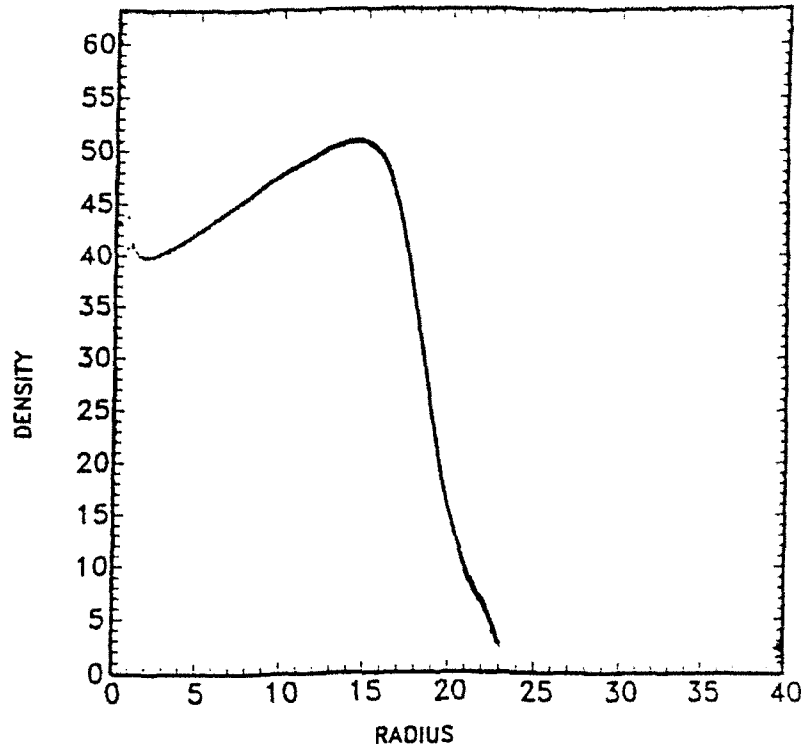
a. 3D spherical implosion at time=48.
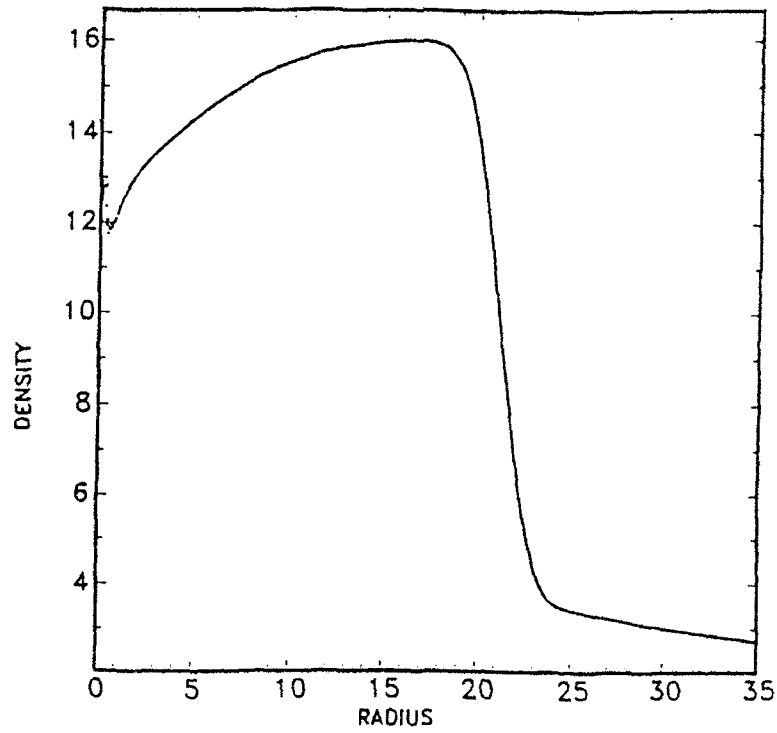

b. 2D cylindrical implosion at time=60.

Figure 1. Density profile for the Noh implosion problem as a function of radius.

model the cylinder. A third reflecting plane represented a perfectly rigid boundary. The initial length of the Iron rod was $Lo=2.54$ cm and the initial diameter was $Do=0.76$ cm. The smoothing length was chosen to be $h=0.076$ cm with 2 particles–per–h in each coordinate direction. A total of 24,455 particles were used. The yield strength (Yo) and shear modulus (μ) of the Iron were taken to be 6 and 0.1 Kb respectively. An initial density of 7.89 g/cc was used. Figure 2 shows the final shape of the computed cylinder (2a) next to a photograph of the experimental [19] article (2b). The the ratio of final length and initial length of the actual experimental rod was $Le/Lo=0.78$. The calculation gave $Lc/Lo=0.79$. The diameter ratios were $De/Do=1.80$ for the experiment and $Dc/Do=1.55$ for the calculation, showing that the simulation has underestimated the bulge near the base of the rod. The calculation required 3 hours of CRAY2 time. This relatively long run time is due to the small impact speed (0.221 km/s) compared to sound speed in iron (4.0 km/s) which controls the time step.

Hypervelocity Impact – Figure 3a shows the SPH calculated debris cloud resulting from the normal impact of a 3 g Copper disk (11.18 mm dia x 3.45 mm thick) on a 2.87 mm thick Aluminum bumper plate at 5.55 km/s. Figure 3b is a radiograph of the actual cloud taken from Piekutowski [20]. The experimental impact was not exactly normal, the Copper disk having a 5.4 deg yaw. We took the smoothing length to be $h=0.20$ mm and 2 particles per h giving 10,000 particles total in the calculation. A Gruneisen equation of state with Copper Hugoniot $Us=0.39+1.5Up$ and Aluminum Hugoniot $Us=0.53+1.5Up$ was used to describe the lead in compression. The shear modulus (μ) and yield strength (Yo) for Copper was taken to be 0.46 Mb and 4.50 Kb respectively. For Aluminum we used $\mu=0.25$ Mb and $Yo=5.50$ Kb. The calculation took 900 cycles and 1.8 c.p.u. hours on a CRAY2. The peculiar shape of the Aluminum debris cloud is captured by the simulation. Figures 3c and 3d show three–dimensional views of the particles. Figure 3c shows only Aluminum bumper plate particles and 3d shows only Copper projectile particles.
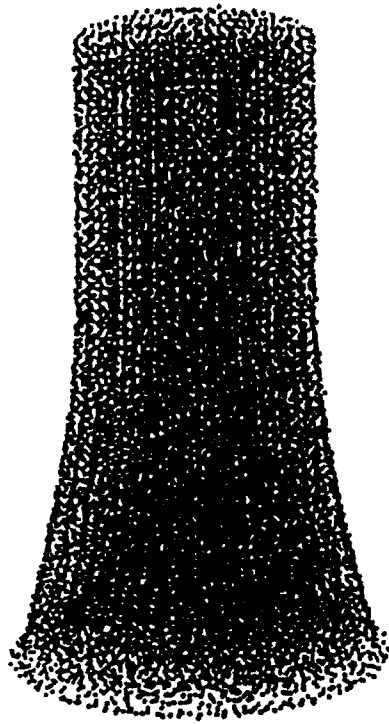
a. Calculation
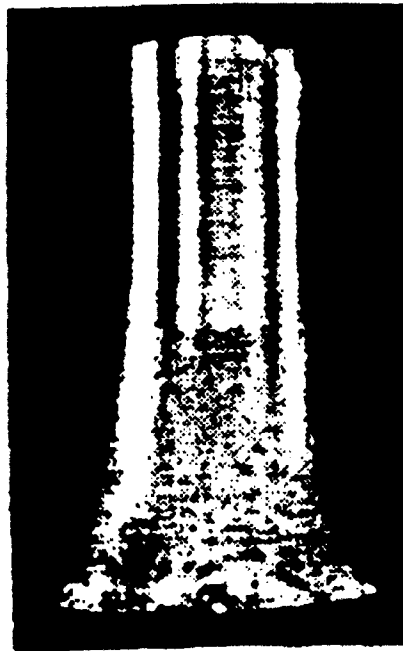


b. Experimental photograph [19].

Figure 2. Cylinder impact test.
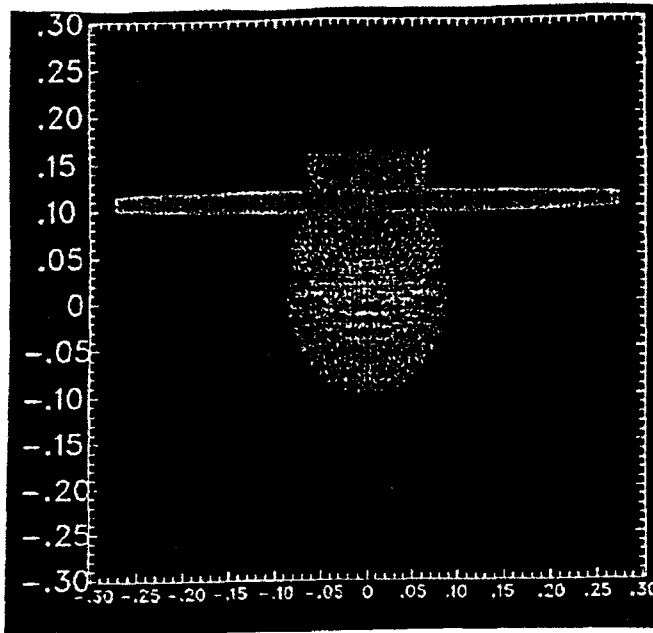
a. Calculation
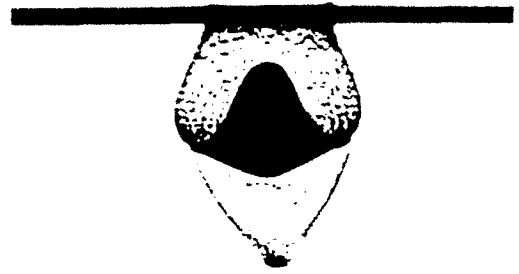
b. Experiment [20]
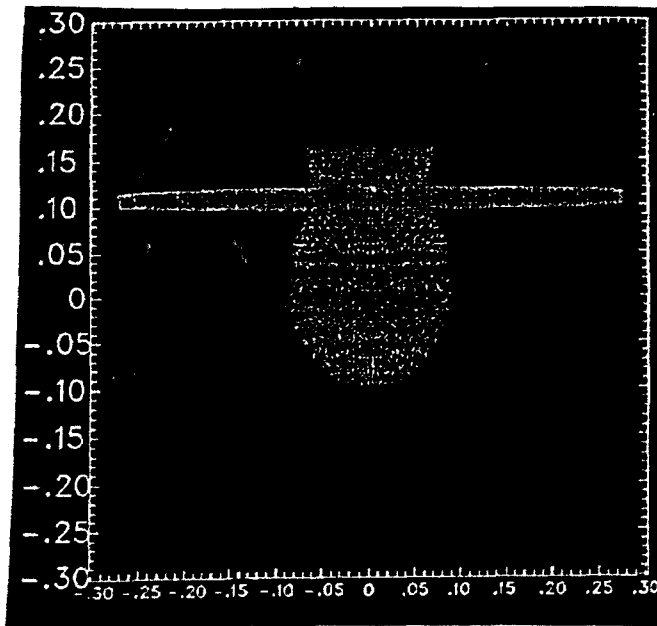
c. Aluminum particles in 3D perspective
(calculation)
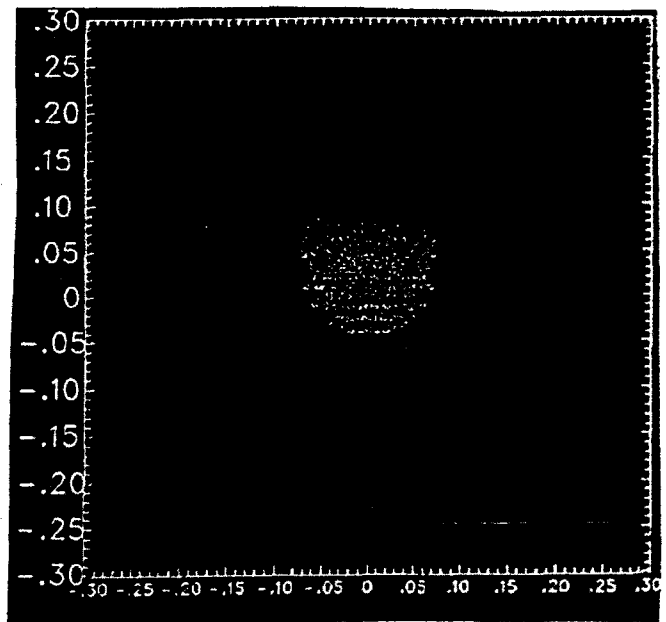
d. Copper particles in 3D perspective
(calculation)

Figure 3. Debris cloud for the impact of a Copper pellet on an Aluminum bumper plate.

18

DISCUSSION

The three-dimensional Smoothed Particle Hydrodynamics code MAGI has been described and three calculations presented. Results of the calculations are in reasonably good agreement with experiment and analysis showing that SPH can be applied to low speed impacts as well as hypervelocity collisions where material strength is unimportant. Advantages of the method are its robustness, conceptual simplicity, ease of adding new physics, a natural treatment of void and the ability to handle high strains in a pure Lagrangian frame. Tracking of debris clouds resulting from hypervelocity impacts is a particularly important advantage of the method. The run times appear to be larger than for Eulerian codes although no direct comparisons have been made. A variable smoothing length formulation of SPH would dramatically improve the running time for the Noh implosion and the lead impact problems presented here. More fundamentally, SPH appears to be readily parallelizable. If so, a one or two order of magnitude speed up is possible on todays massively parallel machines. This is an important area of research.

REFERENCES

1. L.B. Lucy, *Astron. J.* **83** 1013 (1977).
2. R.A. Gingold and J.J. Monaghan, *Mon. Not. R. astr. Soc.* **181**, 375 (1977).
3. R.A. Gingold and J.J. Monaghan, *J. Comput. Phys.* **46, 429** (1982).
4. J.J. Monaghan and R.A. Gingold, *J. Comput. Phys.* **52**, 374 (1983).
5. J.J. Monaghan, *SIAM J. Sci. Stat. Comput.*, **3**, 422 (1982).
6. J.J. Monaghan, *Comp. Phy. Rev.* **3**, 71 (1985).
7. W. Benz, *Numerical Modeling of Nonlinear Stellar Pulsation: Problems and Prospects*, (Kluwer Academic Publishers, Boston Mass, 1990), p.269.
8. J.J. Monaghan, *Computer Physics Reports*, (North Holland Publishers, Amsterdam, 1985), p.71.
9. J. von Neumann and R.D. Richtmyer, *J. Appl. Phys.* **21**, 232 (1950)
10. W.F. Noh, *J. Comput. Phys.* **72**, 78 (1978).
11. J.J. Monaghan, *Preprint Dept. of Math.*, *Monash University, Clayton, Vic.* 3168 (1990).
12. C. Truesdell and W. Noll, in *Handbuch der Physik*, vol III part 3 (S. Flugge, ed., Springer, Berlin, 1965), p.42,44
13. W. Herrmann, *Proceedings, 3rd Int. Conf. on Constitutive Laws for Engineering Materials, Tucon AZ, 1991.*
14. L.D. Libersky and A.G.Petschek, in *Proceedings, The Next Free Lagrange Conf., Jackson Hole, WY 1990*, edited by H.E. Trease, J.W. Fritts and W.P. Crowley (Springer–Verlag, New York, **395** 1991).
15. G.R. Johnson and W.H. Cook, in *Proceedings, Seventh International Symp. on Ballistics, The Hague, The Netherlands*, April 1983).
16. J.C. Lattanzio, J.J. Monaghan, H. Pongracic and M.P. Schwarz, *Mon. Not. R. astr. Soc.* **215**, 125 (1985).
17. R.W. Hockney and J.W. Eastwood, *Computer Simulation Using Particles*, (McGraw–Hill, New York, 1981).
18. R.A. Stellingwerf, in *Proceedings, The Next Free Lagrange Conf., Jackson Hole, WY 1990*, edited by H.E. Trease, J.W. Fritts and W.P. Crowley (Springer–Verlag, New York, **395** 1991).
19. G.R. Johnson and T.J. Holmquist, *J. Appl. Phys.* **64**, 3901 (1988).
20. A.J. Piekutowski, *Int. J. Impact Engng.* **10**, 453 (1990).